Active slab design by lab tests and modelling

Stefano Avesani – Eurac Research, Bolzano, Italy
Daniel Neyer – University of Innsbruck, Innsbruck, Austria
Paolo Baldracchi – Eurac Research, Bolzano, Italy
Ulrich Filippi Oberegger – Eurac Research, Bolzano, Italy
Roberto Lollini – Eurac Research, Bolzano, Italy

The design of a prefabricated active slab for heating and cooling has been supported by lab tests and simulations. The aim was to find performance indicators of an active concrete slab for different reference office rooms and climate conditions. Control strategies in terms of radiant circuit mass flow, inlet temperature, room set point, and temperature deadband have been assessed regarding indoor thermal comfort and energy demand of the investigated thermal zones. The work has given the possibility to test and simulate the behaviour of the slab and to assess the approaches. The methodology consisted of the following steps: (i) design with one-dimensional finite difference models of a pipe heat exchanger, lumped parameter models in TRNSYS and a three-dimensional finite element (FE) model, (ii) first prototype realization and lab test, (iii) refinement and validation of the models according to lab test results, and (iv) parametric studies on reference rooms. Tests have been performed with a double climatic chamber (ISO 8990) connected to an external hydraulic circuit simulating the energy generation system. The models have been used to calculate transient and steady-state temperature and heat flux fields. The FE model consists of the slab with the inlet fluid temperature as step forcing function. Parametric studies of the hygrothermal behaviour of two adjacent rooms have been performed in TRNSYS using reference weather files of three climates, four room geometries and four thermal loads. For each boundary condition, several temperature deadbands and inlet temperatures have been considered. A performance database has been created supporting companies and engineers in components sizing for integration in HVAC systems and optimization of control strategies depending on internal and external loads.

1. Introduction

Low temperature radiant slab technologies match the challenge of energy demand reduction and exploitation of renewable energy in terms of performance and costs (Koschenz M., 2000). Low temperature and buffering of peak loads advance the usage and efficiency of renewable technologies such as solar thermal systems and heat pumps. The use of radiant systems has been spreading since their first commercial installations in the 80's, so that today many products are on the market. The possibility of integrating the radiant circuit already during the prefabrication phase enhances working precision and ease of installation. On the other hand, some structural constraints do not offer much flexibility in the radiant system design such as the position of the coil within the prefabricated slab. In the literature, many studies deal with improvements in modelling and testing of radiant systems (Sattari S., 2006; Karlsson H., 2006; Ferkl L., 2010; Okamoto S., 2010; Al-Othmani M., 2009; Tian Z., Love J.A., 2009). The suitability of simplified models depends mainly on geometry and operation parameters of the system, such as the mass flow rate. On the other hand, detailed models involve strongly coupled space and time dependent physics and are therefore complex to develop and computationally expensive.
Goals of the work have been: the support of a company in the design and optimization of a prefabricated radiant slab, the provision of standard performance figures for the built product, and the development and assessment of control strategies. In this paper, a critical overview of methodology and results is given.

2. Methods

The methodology has been based on simulations and lab tests. First, the slab's thermal behaviour was tested in the lab. Next, numerical models were calibrated according to test results and known parameters. Finally, the models were run to predict the slab's thermal performance under the design boundary conditions.

Several models have been built depending on the design goals. Preliminary design was based on a simplified one-dimensional (1D) finite difference model (FDM). 3D Finite Element Models (FEM) were used for the calculation of the temperature field and heat fluxes fields under steady state standard boundary conditions as described in the UNI EN 1264 (UNI EN 1264, 2009); the slab operation modes were computed and evaluated with TRNSYS for four reference offices (single, double, open office and meeting room) in three different climates (Bolzano, Brunico and Venice). Lab measurements provided both steady-state and transient values, FEM models were run only in steady-state and TRNSYS simulations gave the transient behaviour of the slab.

2.1 Description of the radiant slab

The radiant system proposed by the company is a concrete prefabricated slab with a hydraulic circuit embedded close to the ceiling. Pipes have an external diameter of 0.02 m and a spacing of 0.15 m. In Fig. and Table , a typical construction is specified.

2.2 Lab test

The active slab was tested within the guarded hot box at EURAC (Giovanardi A., 2010). The lab is equipped with two fully instrumented climatic chambers, one external hydraulic circuit (providing water at desired temperature and mass flow), and a solar simulator (not used in this case). The testing concept consisted in maintaining constant boundary conditions on the surfaces of the sample and in feeding the hydraulic circuit with a controlled water temperature and flow, considering both winter (heating) and summer (cooling) conditions. The aim of the tests was to measure the surfaces' heat fluxes through the ceiling and floor and their temperatures. Measurements both of the initial and final steady-states and of the transient period between these two were performed. Tests with step function boundary condition were carried out according to the following procedure: (i) keeping constant boundary conditions at the slab surfaces (air velocity and temperature) and constant fluid flow rate and temperature; (ii) step variation of fluid flow and temperature; (iii) achievement of steady-state after a step variation of the fluid inlet temperature.

Table 2 summarizes the tests carried out and the imposed boundary conditions. During all tests, the variables reported in Table 3 were measured.

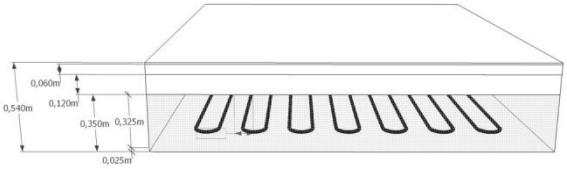

Fig. 1 – Active slab with coil close to the ceiling.

MATERIAL	LAMBDA/RHO/CP	THICKNESS
Name	[W/mK]/[kg/m³]/[J/kgK]	[m]
Concrete	2.1 / 2500 / 840	0.025
Pipeline PEX	0.35 / 938 / 1000	0.02
Concrete	2.1 / 2500 / 840	0.025 + 0.28
Lightweight concrete	0.08 / 350 / 400	0.12
Screed	1.4 / 2150 / 840	0.06
Floor	1.5 / 2300 / 1000	0.01

Table 1 – Slab construction from bottom (ceiling) to top (floor).

	T air [°C]	**T inlet fluid** [°C]	**Mass flow** [l/h]
H	20	From 20 to 25	113
H	20	From 25 to 35	113
C	26	From 26 to 22	113
C	26	From 22 to 17	113
H	20	23 (first 6 hours) and 25 (second 6 hours)	113 on/off
H	20	25	113 ± 20%

Table 2 – Test conditions of the slab (H: heating conditions; C: cooling conditions).

Although the active slab is a horizontal building element, it was tested in a vertical position, the only one allowed by the setup of the guarded hot box. However, both climatic chambers, hot and cold, were set up in order to reproduce reliable boundary conditions controlling the temperature and keeping the velocity of the airstreams directed on the target surfaces constant.

Variable	Sensor type	Position
Slab surface temperatures	Thermo couples	16 points on the ceiling, 9 points on the floor
Internal chamber surface temperatures	Thermo couples	9 per chamber
Heat fluxes	Heat plate (0.49 m x 0.49 m)	1 for the ceiling and 1 for the floor
Chamber air temperatures	Pt100	9 sensors per chamber
Mass flow	Electromagnetic meter	1 in the hydraulic circuit
Water temperatures	Pt100	1 at the inlet and 1 at the outlet of the hydraulic circuit

Table 3 – Lab measurements' points and sensor typology.

The heat flux through the floor surface was directly measured with the heat plate as measured temperatures on the floor surface differ by less than 0.3 K - therefore also the heat flux through it can be considered homogeneous. The same procedure could not be applied for the ceiling due to the inhomogeneity of the heat flux near the coil. Hence, the ceiling heat flux at steady state conditions was calculated as the difference between the total heat flux transferred from the fluid to the slab and the heat flux measured at the floor. Radiant and convective surface heat transfer coefficients were estimated for both floor and ceiling using surface (floor, ceiling, and chamber wall) and air temperatures, air velocity, and heat plate measurements.

2.3 FEM model

The aim of developing a FEM model was to evaluate the slab thermal performances (i) under steady-state reference boundary conditions (as stated in the norms), (ii) both for the tested specimen and for the maximum slab dimensions (respectively 2.4 m times 2.4 m and 6 m times 2.4 m), and (iii) for different mass flow rates. A 3D FEM model was set up in COMSOL, coupling heat transfer in solids and fluids with fluid dynamics. The model was validated with lab data as explained afterward.

The FEM model consists of two steady-state de-coupled submodels with Dirichlet boundary conditions at the internal surface of the pipe determined iteratively. In Submodel A, the 3D heat transfer in solids was solved on the material layers (one cuboid for each material) and on the pipeline (linear extrusion of an annulus). In Submodel B, the pipe was considered stretched, without curves. Hence, a 2D rectangle was set as the domain to which the equations of fluid dynamics and fluid heat transfer were applied. The hypothesis of axial symmetry at the pipe centre was used. Moreover, the pipe thickness was modelled just in 2D as a rectangle as well. The link between Submodel A and Submodel B was performed imposing the temperature calculated in the other Submodel at the common interface (cylindrical pipe surface for the 3D Submodel A and line 7 for the 2D Submodel B - Fig. 2).

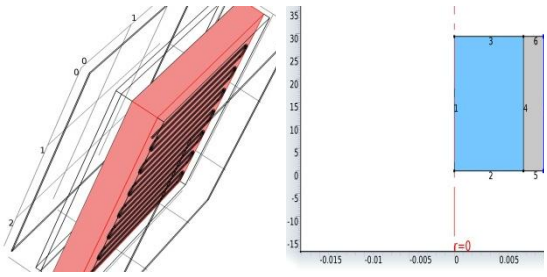

Fig. 2 – 3D slab model without pipe (left). 2D pipe model symmetric on the pipe centre axis (x axis = radius, y axis = length): highlighted the boundary condition on line 7 interface between the 2D and 3D models (right).

Steady-state 3D heat transfer in solids (Submodel A) is governed by Equation 1:

$$\nabla \cdot (\lambda \nabla T) + \dot{Q} = 0 \qquad (1)$$

Steady-state 2D fluid dynamics and heat transfer in fluids (Submodel B) is described by Equations 2 and 3:

$$\rho(\boldsymbol{u}\cdot\nabla)\boldsymbol{u} = \nabla\cdot[-p\boldsymbol{I} + \mu(\nabla\boldsymbol{u} + (\nabla\boldsymbol{u})^{\mathrm{T}})] \quad (2)$$

$$\rho c_p \boldsymbol{u}\cdot\nabla\mathrm{T} = \nabla\cdot(\lambda\nabla T) + Q \quad (3)$$

Model boundary conditions were set as follows. For Submodel A, the surface heat transfer coefficients, surface emissivity and ambient and boundary surfaces' temperatures were kept constant at the slab's bottom (ceiling) and top (floor) surface, while adiabatic conditions were assumed along the slab's lateral surfaces. For Submodel B, inlet fluid velocity and temperature as well as outlet pressure were kept constant.

The mesh was generated featuring a fine grid in the most critical regions (especially at the fluid-solid interfaces and in the volume of the pipeline) and a coarser one where large gradients of temperatures were not expected - due to the high thermal resistance from the pipe plane to the floor.

Boundary conditions were: the fluid inlet temperature and mass flow, the reference pressure at the fluid outlet (2D model), the temperature at the solid interface between pipe and concrete (2D and 3D model), the convective heat exchange coefficient on the ceiling and floor surfaces, the reference ambient air temperature, the infrared emissivity of the ceiling, the floor and the two reference boundary surfaces parallel to them (3D model). For these two planes the surface temperature was also set. All other boundary surfaces have been set adiabatic.

The FEM model was validated by comparing steady-state surface heat fluxes and temperatures and outlet fluid temperatures with the respective test outputs. Hence, lab boundary conditions were set in the FEM simulations and the surface emissivity and convective heat transfer coefficient of the surfaces tuned until an agreement between the two was reached. Outputs of the model are 3D fields of surface temperatures and heat fluxes and outlet fluid temperature.

2.4 TRNSYS Model

TRNSYS 17.1 was used to estimate the yearly performance of the activated slab for different usage profiles, control strategies, and climates. The model of thermo-active building element (Koschenz et al., 2000) avoids the complex and computationally expensive FE calculations, nevertheless allowing yearly performance estimates. The 2D solution of the heat conduction differential equation can be represented by a network of resistances. This model has strong geometric limitations (TRNSYS 17.1, 2012). Therefore, a workaround was devised and tested in order to overcome these restrictions. Construction properties were manipulated so that all geometric and resistance criteria were fulfilled and the resulting heat fluxes and surface temperatures match the lab test results. To find these properties (density, heat capacity, conductivity, and the thickness) a two-thermal zones model simulating the hot box setup (vertical slab separating left and right chambers) was created. Lab boundary conditions (air temperature inside the chamber, the chamber internal surfaces' temperatures, and the air speed along the slab) were used. By tuning the radiative and convective heat transfer coefficients and entering measured fluid inlet temperatures into the model, the deviation between measured and simulated fluid outlet and slab surface temperatures was minimized. The properties used in the following simulations are a tube wall thickness of 0.045 m, a conductivity of 4.2 W/(mK), a capacity of 420 J/(kgK) and a density of 1250 kg/m³. Infrared radiation was modelled with the TRNSYS detailed model based on view factor. Heating and cooling demand were calculated based on the fluid temperatures. The parametric study performed in TRNSYS considered different thermal zone geometry, ventilation rates, and internal loads. For the yearly simulations, four different profiles were defined based on the Swiss standard SIA 2024 (SIA 2024, 2006). They were applied to each of the following reference rooms: single office, double office, meeting room, and open space office. The lighting schedule is further multiplied by an on/off control signal. In the following, the relevant boundary conditions are exemplified for the double office room.

The arrangement of the reference rooms was chosen such that the influence of up- and downward directed energy fluxes could be studied. Both rooms were treated in the same way (internal loads and temperature setpoint), leading to a two thermal zone

one over the other, with only one external wall and one window per zone. Some other important boundary conditions are explained in Table 4.
As a control strategy, a simple on/off controller was chosen. The effect of different deadbands and temperature setpoints were studied. A graphical explanation of the working of the controller can be found in Fig. 3 with heating and cooling setpoints equal to 21°C and 26°C, respectively, and a deadband of 1 K for heating and cooling.
The operative temperature (simplified as the average of radiation and air temperature) was used as an input variable to the controller.

3. Results

3.1 Standard steady state and dynamic performance figures

The lab test and FEM simulations gave steady state performances at lab and normed boundary conditions (UNI EN 1264), respectively. Energy performances were assessed in terms of surfaces' heat fluxes against logarithmic temperature differences between water and ambient temperatures. Heat flows mainly through the bottom surface, as the thermal resistance of the layer delimited by coil and top surface is much higher (Rceiling = 0.011 m²K/W, Rfloor = 1.7 m²K/W). In fact, the rate between ceiling and floor specific heat flux is more than 15. In Figure 4 both lab test and FEM simulations results are reported. Ratios between heat flux and logarithmic difference of temperature are 6.5 and 4.6 in heating, 5.7 and 6.2 in cooling for lab and FEM respectively.

Name	Specification
Climate/ weather	Bolzano, Brunico, Venice (IT) Source (METEONORM 7)
Constructions / orientation	South surface "external", all inner walls "adiabatic", radiant slabs with "active layer" (Table) between zones
Windows	U-value 0.61 W/m²K, g-value 0.402, TRNSYS window ID 13004, area 60% of total wall surface
Shading	External, fc = 0.4; on if I > 140 W/m² and off if I <120 W/m² on the receiver
Ventilation	n = 36m³/(h p), Tsupply min 18°C, max 26°C
Infiltration	n50 = 1.5 air changes per hour
Internal gains	According to SIA 2024
Persons	According to SIA 2024
Light	According to SIA 2024, plus: off if I >140 W/m², on if I < 120 W/m²
Supply temp. heating/cooling	Parametrically changed, but constant during each simulation; 30°C, 28 °C, 26 °C for heating / 15°C, 17°C, 19°C for cooling
Active layer geometry	Geometry shown in Figure 1

Table 4 – Table of TRNSYS boundary conditions used

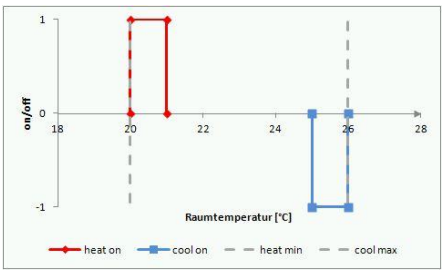

Fig. 3 – On/off controller with deadbands and temperature setpoints

Surface temperatures were also measured and evaluated from the point of view of radiant discomfort. Ceiling and floor temperature differences were compared with the comfort classes' limits suggested by (EN ISO 7730). For a fluid inlet temperature of 35°C, the average surface temperature difference between ceiling and floor at the steady-state condition goes up to 5 K (Fig. 5).
In FEM simulations, after validation, standard boundary conditions according to EN 1264 were set in order to provide the slab thermal performances as required by that norm. Results are reported in Fig. 4, Fig. 6 and Fig. 7. The ceiling surface has the higher temperature gradients all over the surface. The maximum temperature difference reaches 7 K and is between the inlet corresponding point (the warmest) and the lower right corner (Fig. 4).
FEM models were used to evaluate the impact of a bigger slab with different mass flow rate on the slab thermal performance. The role of the mass flow rate is to assure adequate heat fluxes through

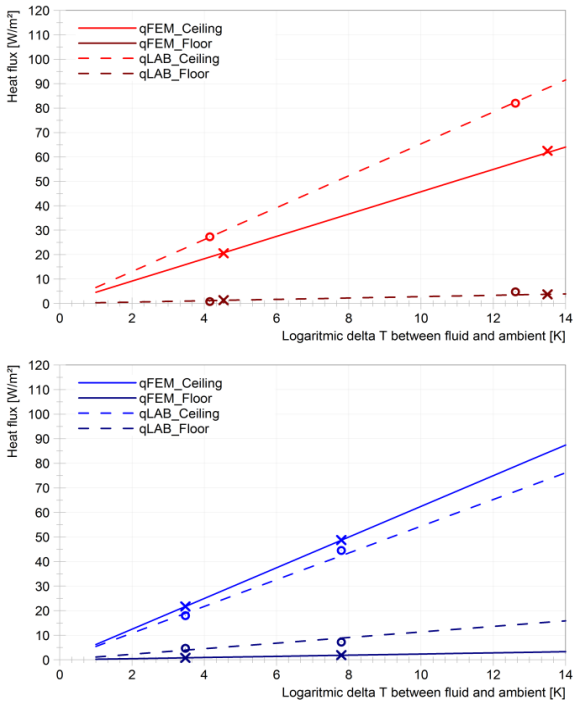

Fig. 4 – Lab test and 3D FEM simulations results in heating (above) and cooling (below).

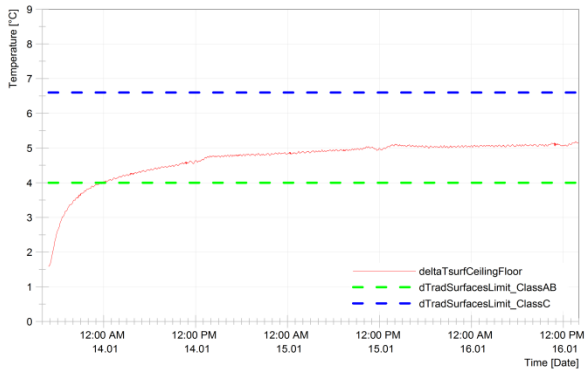

Fig. 5 – Measured temperature difference between ceiling and floor in heating mode in time. Temperatures averaged over the sample surface.

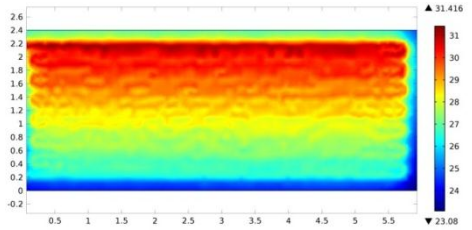

Fig. 6 – FEM steady-state ceiling surface temperatures: inlet fluid temperature 35°C; mass flow rate 113 kg/h; slab dimensions 2.4 m times 6 m.

the surfaces and fluid inlet-outlet temperature differences of at most 5 K (as recommended by design). Hence, a comparative assessment of the heat fluxes has been performed (Fig. 7). For a bigger slab, differences are not relevant (< 2 W/m²). Nevertheless, for a bigger slab the inlet mass flow plays a role impacting with ±15 W/m² for a mass flow rate doubling/halving.

The time-dependent thermal response of the slab was measured in the lab. Fig. 5 shows the time range between two steady-states - the initial condition at 20°C and the final conditions with fluid inlet temperature of 35°C and surface heat fluxes constant in time. Nevertheless, steady-state conditions will never be realized in a system installed in an actual building as the normally employed control strategies are based on thermal charging and discharging of the concrete depending on the setpoints and on the real (dynamic) boundary conditions. Therefore, heat fluxes through the slab surfaces were also evaluated in an on-off test, in which the circulating pump was periodically switched on and off every three hours representing a possible control strategy. After three hours, more than 50% of the steady-state power had been reached (Fig. 8).

Even if the slab thermal response is quite slow (time constant of 6 h with driving temperature difference between fluid inlet temperature and environment of 5°C), the high thermal inertia of the system delivers a satisfactory amount of energy to the ambient also when the pumps are off (90 Wh/m² for fluid inlet temperature of 25°C).

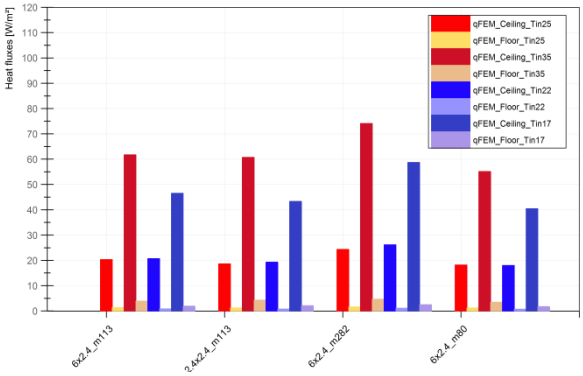

Fig. 7 – Parametric analysis of active slab: slab dimensions and inlet fluid mass flow vary.

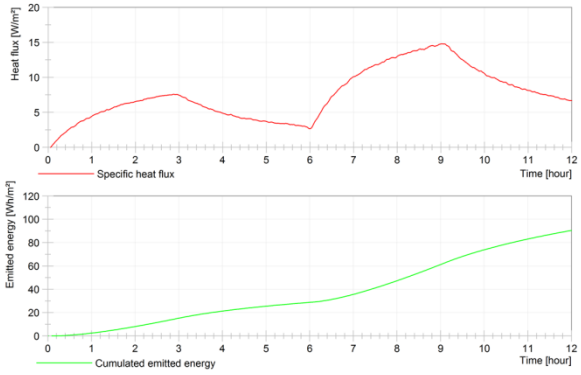

Fig. 8 – Radiant heat and energy at the ceiling surface obtained in a 12 hours lab test (heating mode) using an on-off based control strategy.

3.2 Energy demand and thermal comfort

Concerning the model accuracy, between lab and TRNSYS results, referring to steady state and dynamic lab tests' and TRNSYS's results in heating and cooling modes, a maximum average deviation of <5% for the fluid outlet temperature, <10% for surface temperatures and <15% for the heat flux directed up- and downwards could be achieved.

The TRNSYS simulation results have been analysed in terms of energy demand for heating and cooling, on-off control cycles, running hours of the pump, and thermal comfort. Results for the Bolzano case are only reported in detail: the Brunico and Venice results are summarized at the end. Hysteresys deadband for the on-off regulation of the slab pumps, fluid inlet temperatures, air setpoints were parametrically changed. The heating and cooling demand increases slightly with an increase of the deadband Fig. 9.

Considering ideal load calculation (no plant) ventilation losses for supplying to the indoor environment with neutral air (20°C in heating and 26°C in cooling) are 24 kWh/m²y and 1.2 kWh/m²y in winter and summer respectively. Transmission losses account for 13.5 and 6 kWh/m²y in winter and summer respectively. Adding the active slab, energy demand varies between 15.3 and 23.8 kWh/m²y depending on the deadbands.

Furthermore, results show that differences in annual energy demands using other supply temperatures (15/30, 17/28, 19/26, and ideal) are less than 1 kWh/(m²y). This is not true for the number of on/off cycles or the running hours. With increasing deadband, the number of on/off cycles decreases. The minimum is at about 20 cycles per year for a deadband of 5 K. The running hours react the other way round but with another trend. A large deadband implies long pump operation until the tripping point is reached.

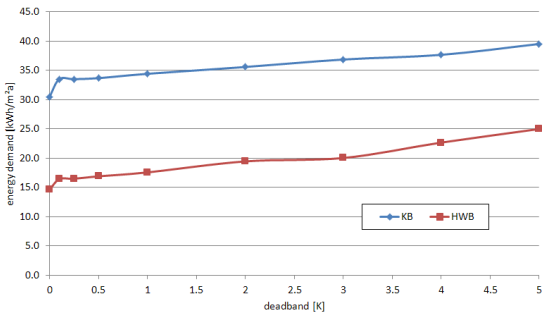

Fig. 9 – Evaluation of the heating (HWB) and cooling (KB) demand for the Bolzano case and different deadbands.

An analysis of the air temperature distribution over a year shows that the output power of the slab, for constant mass flow and temperature of the fluid, is high enough to reach the minimum and maximum required temperatures – also for other fluid inlet temperatures. Minimum and maximum allowed temperatures (20°C and 26°C) are actually always respected (Fig. 11).

The thermal comfort analysis was done based on the Predicted Mean Vote (PMV) as defined in the ISO 7730 (EN ISO 7730, 2006) and in (Fanger P.O, 1982). One representation is shown in Fig. 12, which reports the time distribution of the PMV over the year for different control deadbands (with constant parameters clo=1, met=1.2, v=0.2 m/s).

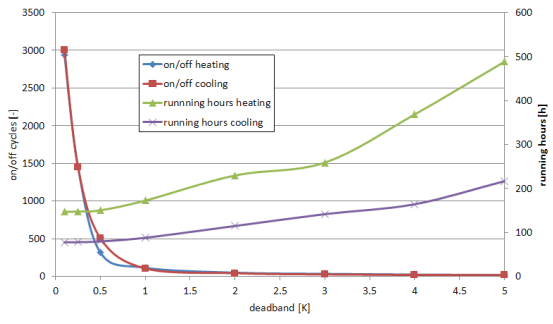

Fig. 10 – Evaluation of pump running hours and on/off cycles for heating and cooling for the Bolzano case and different deadbands.

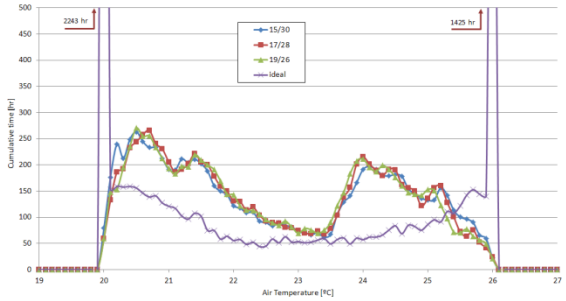

Fig. 11 – Evaluation of the temperature distribution over a year for the Bolzano case and different supply temperatures.

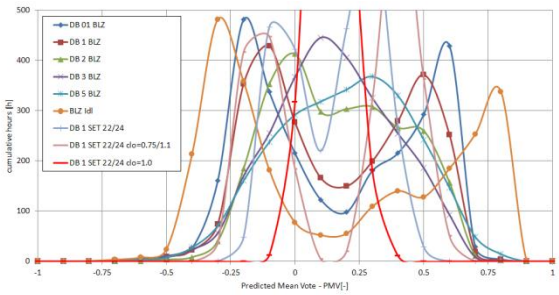

Fig. 12 – Evaluation of the thermal comfort in terms of cumulated number of hours of use of the system in a year for different deadbands and setpoints during which the PMV has the indicated value.

Only the right hand PMV peaks for ideal system (no deadband), 0.1 K and 1 K deadband are outside the allowed class B (maximum of 10% thermally dissatisfied people and PMV ±0.5 (EN ISO 7730)).

Analogous simulations have been performed for other climates (Venice and Bruneck in Italy) as well. Moreover, extremes like sudden temperature drops or bad architectural solutions (excessive glazing) have been analysed.

Concerning Venice's humid climate, simulations have been done both with and without humidity control systems. Without any strategy against condensation apart from standard on-off pump control, in the Venetian climate, for defined ventilation rates and internal loads, condensation occurred after 7.5 hours equivalent to 30 simulation time steps. Increasing the supply temperature from standard 15°C up to 19°C reduce the number of condensing hours, but not eliminate it.

In the extreme conditions mentioned above, no problems with the heating and cooling power supply occurred. Neither for the extreme glazing (80% of the external wall surface) in combination with an extreme profile for a meeting room (internal and external loads, simultaneously), nor for an outdoor temperature drop of ±10 K (leading to outdoor air temperatures around -20°C/+40°C), the maximum power limits have been reached.

4. Conclusions and discussion

In this paper the methodology used to model and test a radiant prefabricated slab are shown together with the achieved results. The following issues have been faced and resolved.

Methodology: Key parameters for the modelling and testing have been the convective heat exchange coefficients, the emissivity and the active surfaces' view factors. If convection and radiation measurements and calculation are not accurate enough, neither the energy demand (heating and cooling), nor the thermal comfort can be predicted reliably. Lab and FEM results have had different purposes: lab tests have been used just to validate the models - as the lab convective heat exchange coefficients could not be changed. FEM simulations have aimed at evaluating the performance at norm boundary conditions, for different slab dimensions, fluid inlet temperatures and flow rates.

Differences in the lab and FEM steady-state performance reported in Fig. 4 are discussed here: firstly values of the surface heat exchange coefficients in lab and in simulations have been different (as reported in Table 5). Secondly, the lab chambers' ambient conditions could not be kept exactly at 20 (and 26) °C in heating (and cooling) mode: the chamber air temperature differed from the set point by a maximum of 0.7 K. The chamber surfaces reached a maximum of 2 K difference with the air setpoint.

Lab: A radiant device was tested in the guarded hot box with the support of a hydraulic circuit with variable fluid inlet temperatures and mass flow rates. Steady-state performances have been measured. Other dynamic tests, such as the on-off control of the circulation pump, were performed and showed interesting results for the evaluation of the slab reaction time. Besides the time constant, the dynamic variation of the heat flux and the released energy based on a three hours on-off

	Laboratory	FEM (EN1264)
	[W/m²K]	[W/m²K]
h radiant[4]	4.8	4.9
h convective	~ 10 - 12 (ceiling heating and cooling) ~16 (floor heating and cooling)	5.5 (heating floor, cooling ceiling) 1.5 (cooling floor, heating ceiling

Table 5 – Surface heat exchange coefficients for lab tests (air velocity flowing on the floor surface is higher than the ceiling) and FEM simulations (convective coefficients from the UN EN 1264)

pump control strategy were measured, offering more useful information for the designers.

Measurements and calculation of the heat fluxes have been performed with different methods. Direct measurements of the heat fluxes (with a 0.4 m times 0.4 m heat plate) and of the temperatures are very sensitive to the positioning of the measuring device on the slab surface, especially for inhomogeneous temperature fields (as caused by the thermoactive coil close to the slab bottom surface). Indirect measurements, based on the energy delivered to / absorbed by the slab, show more robustness.

FEM: FEM models' results were very useful for detailed evaluation of the space temperature fields which have deep implication in the thermal indoor comfort assessment (Fig. 6). Nevertheless, simplifications in the modelling approach and in the mesh choice have to be carefully considered balancing between model reliability and usability. As an example, surface temperatures fluctuations of Fig. 6 are mainly due to a too coarse 3D mesh. These steady-state calculations needed a simulating time in the order of 0.5 hours with a 4 core 16 Gb RAM calculator. Time-dependent 3D FEM models were not used because of the unaffordable calculation time without further model simplification.

TRNSYS: Simplified models - such as the TRNSYS model - have some strong limitations, but work well within clearly defined ranges if tuned with measurement data.

The radiant slab: The studied thermo active slab shows a good performance in terms of power, energy and thermal comfort if it is combined with a mechanical ventilation system that can supply neutral air to the indoor environment. In fact, the active slab can cover the transmission losses and the part of the ventilation losses not covered by the heat recovery system, resulting in an heating energy demand of circa 18 kWh/m²y for a deadband of 0.5 K. The increase of the energy demand with the deadband Fig. 9 can be explained by an overheating or overcooling up to a certain level before the system is switched off.

Power peaks covering was verified simulating unfavourable climate conditions and building features. Nevertheless, setpoint temperatures could have been kept because the simulated air conditioning system had enough power to supply air at adequate temperature. The slab provides the base load and the air conditioning system the peak load (like the sudden temperature drop).

Considering global indoor comfort, PMV time frequency over the year changes with the increasing deadband, from two peaks (corresponding to the two setpoint – heating and cooling) on both sides to a single peak (Fig. 12). This is mainly because the heating and cooling setpoints have not been optimised – just fixed at 20°C and 26°C. If the setpoints and the clothing factors were optimised, an ideal distribution could be reached with a setpoint of 22/24°C and a clothing factor of one.

As is clear in Fig. 5, floor-ceiling temperature difference could have an impact on the radiant asymmetry local discomfort switching from comfort class A-B and to C in case of high fluid inlet temperature (35°C) and standard mass flows (19 kg/m²h).

Dynamic tests show that the slab reaction time is low in terms of time constant; nevertheless, simulations have allowed to verify the low risk of overheating and overcooling with a correct on-off control strategy.

Considering the active slab key parameters, the main differences in heat fluxes and surface temperatures are caused by varying the mass flow rate (just for a bigger slab), while slab dimensions have less influence on the results for a well-

[4] Linearized radiant coefficient

designed mass flow. On the one hand, a bigger slab means a longer coil and more heat losses along it.A bigger slab means less influence of boundary effects on pipe heat transfer. The mass flow rate plays an important role in controlling the fluid inlet-outlet temperature difference and the resulting surface temperatures that in turn determine the heat fluxes.

To avoid condensation in humid climates, either the supplied air can be dehumidified, or the slab surface temperature has to be kept above a certain level. This can be done using a higher supply temperature or a control strategy that switches the cooling off before the surface is getting too cold. With condensation occurring only during few hours, and keeping hydrothermal comfort conditions throughout the year in a reasonable range, a shutdown of the cooling system could be sufficient.

5. Nomenclature

T	Temperature [K]
u	Velocity [m s^{-1}]
p	Pressure [Pa]
Q	Heat flux [W]
F	Volume forces [N m^{-3}]
Cp	Specific heat [J kg^{-1} K^{-1}]
μ	Dynamic viscosity [Pa s]
ϱ	Density [kg m^{-3}]
λ	Conductivity [W $m^{-1}K^{-1}$]

References

Koschenz M., Lehmann, B., 2000, Handbuch Thermoaktive Bauteilsysteme TABS, EMPA Energiesysteme / Haustechnik, Dübendorf Schweiz.

METEONORM 7, www.meteotest.ch, (last accessed November 2nd 2012).

TRNSYS 17.1, The Transient Energy System Simulation Tool, www.trnsys.com, (last accessed November 2nd 2012).

SIA 2024, Merkblatt 2024: Standard-Nutzungsbedingungen für die Energie- und Gebäudetechnik, schweizerischer Ingenieur- und architektenverein, Zürich, 2006

Fanger P.O., 1982, Thermal comfort, analysis and applications in environmental engineering, Reprint. - Malabar, Fla.: Krieger

EN ISO 7730, 2006, Ergonomics of the thermal environment

UNI EN 1264, 2009, Water based surface embedded heating and cooling systems

Sattari S., 2006, A parametric study on radiant floor heating system performance, Renewable Energy 31 (10) (2006) 1617–1626

Karlsson H., 2006, Thermal system analysis of embedded building integrated heating: numerical model and validation of hydronic floor heating systems, Chalmers Reproservice, Sweden

Okamoto S. et al., 2010, A simplified calculation method for estimating heat flux from ceiling radiant panels, Energy and Buildings 42 (1) (2010) 29–33

Ferkl L., Sirok J., 2010, Ceiling radiant cooling: comparison of ARMAX and subspace identification modelling methods, Building and Environment 45 (1) (2010) 205–212

Al-Othmani M. et al., 2009, Experimental and Theoretical study of transient human thermal comfort response in convective and radiative environments, HVAC&R Research 15 (5) (2009) 855–873.

Tian Z., Love J.A., 2009, Energy performance optimization of radiant slab cooling using building simulation and field measurements, Energy and Buildings 41 (3) (2009) 320–330

A. Giovanardi, P. Baldracchi, R. Lollini, 2010. A new test rig for the assessment of building envelope components integrating solar active systems. Eurosun - International Conference on Solar Heating, Cooling and Buildings, Graz